LHCb 2000-90 VELO
10th October 2000

VELO Geometry Optimisation

T. Bowcock, M. McCubbin and C. Parkes
University of Liverpool
H. Dijkstra, F. Fiedler, B. Hay, T. Ruf
CERN, Geneva
N. van Bakel, J. van den Brand, M. Ferro-Luzzi
NIKHEF, Amsterdam
T. Ketel
Vrije Universiteit, Amsterdam
P. Koppenburg
Universite de Lausanne

Abstract

New possible layouts of the LHCb Vertex Locator (VELO) have been compared with the existing baseline design outlined in the Technical Proposal. Based on a comparison of essential figures of merit, namely vertex resolutions, event selection efficiencies, trigger performance, and technical constraints an updated baseline design is proposed. The new design retains the same number of electronic channels as that in the Technical Proposal, but has an increased number of measuring stations (25 rather than 17) with a reduced inner radius (8mm rather than 10mm).

Contents

1 Introduction

The design of the VELO is critical to the successful operation and exploitation of the data from LHCb. Primarily the detector must be capable of providing high resolution information on displaced secondary vertices, which are a distinctive feature of b-hadron decays. This information will be a vital element of the L1 trigger as well as the offline analysis. The design of a suitable detector, as a series of forward disks, was outlined in the Technical Proposal (TP) [1]. The design was substantially complicated by the need to place it close to the interaction point to enable good primary and secondary vertex resolution. This implied the sensors must be retractable (during injection) and be extremely radiation tolerant. In addition, the VELO must not compromise the performance of the remainder of the experiment. The introduction of unecessarily large numbers of forward disks adds subtantially to the cost and complexity of the VELO and could introduce large amounts of material before the RICH, tracking chambers and calorimeters.

The aim of this study was to test the expected outcome of making modifications to the existing baseline design of the VELO detector. The effects of increasing the numbers of measuring stations, of changing the sensor resolution and of using more realistic models of the RF shields were quantified.

2 Requirements and Constraints

The Technical Proposal VELO design consisted of a series of 17 disks within a vacuum vessel approximately 1 metre long. Each disk was instrumented with two planes of silicon sensor, one plane designed to measure radial position coordinates (r-detectors) and the other to measure azimuthal coordinates (ϕ-detectors). The detector prototypes had strips which were inclined by a few degrees from the purely radial to resolve ambiguities. To make the detectors as radiation tolerant as possible, n-strip in n-bulk technology was chosen [2]. In addition, the choice of thin (150μm) Si sensors was made to decrease the depletion voltage[1] and lower the bulk leakage currents; this as a consequence reduces the expected signal.

Since the submission of the Technical Proposal substantial progress has been made in the understanding of the damage to Si detectors, and this, together with new estimates of the flux, enables us to envisage the use of slightly thicker Si closer to the interaction point. For example, a reduction in the inner radius of the detectors from 10mm to 8mm could improve the measurement of the impact parameter of a track by up to 20%. To benefit further from the "lever-arm" effect a reduction in strip-pitch is necessary. However, a simple reduction in the inner radius implied an increase in the overall number of channels over the original baseline design. In order to keep the cost of the electronics from rising substantially it was decided to impose the constraint that the number of electronic channels (readout strips) remain approximately constant. This implied a redesign of the detector strip-pitch as a function of radius and of the outer radius of the sensor.

In addition to considerations of the sensor's performance important constraints are

[1]The depletion voltage, V_d, is approximately proportional to the square of the thickness of the sensor, $V_d \propto d^2$.

placed on the possible designs by the twin requirements of the sensors being within their own secondary vacuum and the need to RF shield the sensors and electronics from the beam.

Below we discuss, in more detail, the overall technical parameters and requirements that inform our optimisation process.

2.1 Geometrical constraints and interaction with the LHC

The VELO detector is the closest to the nominal interaction point at $z = 0$. It occupies the region between 20cm upstream (z=-20cm) to 80cm downstream (z=80cm). All the VELO sensors, their front-end electronics, and two additional planes of "pile-up" counters are contained within a vacuum tank that spans this region. These active elements are separated from the primary machine vacuum and beam by a thin wall. As an additional safety requirement the thickness of this wall must be sufficient not to rupture if a small differential pressure between the secondary and primary vacuum is established [3]. This wall introduces material between the primary interaction point and the measuring stations degrading, through multiple Coulomb scattering, the resolution of the vertex reconstruction. The effects of introducing this material are part of the reoptimisation procedure.

2.2 Wake field suppression

In addition to the vacuum requirements it is necessary to introduce wake field suppressors to guide the mirror charge and limit the RF power dissipation close to the sensors. This is necessary to avoid a large heat load being placed on the detectors and to shield the sensitive electronics from noise.

Two approaches have been considered. In the first, the detector stations are individually enclosed in thin-walled Al caps. This design, first put forward in the Technical Proposal, minimises the amount of Al seen by particle tracks before the first tracking point. However, because the caps form cavity-like structures, this design requires a dedicated wake field suppressor in the vicinity of the beams [4]. Therefore, it was suggested to use a number (e.g. four) long and thin-walled strips spanning the LHCb VELO setup, similar to what is used in the Hera-B setup [5]. These strips, being almost parallel to the particle tracks, must be substantially thinner than the Al enclosures.

In the second approach (see e.g. [6, 7]), the detector stations are encapsulated in a single Al box (per top/bottom half). The enclosure is corrugated to accomodate for the dent (across the LHC plane) of the detector modules. The central section of the encapsulation, which is first traversed by the tracks, is shaped to minimise multiple scattering (deeper corrugation). This corrugation should not be too deep, since the Al enclosure, which is primarily needed as a vacuum separation, must act as well as wake field suppressor. The limits on the corrugation depth are dictated on the low side by multiple scattering effects, on the high side by wake field effects.

The two designs can be compared. Although the TP design does provide for better vacuum pumping in the section close to the beams, which helps reduce possible dynamic vacuum phenomena, the use of long, thin, wake field suppressor strips has a number of disadvantages:

- The affordable thickness of the strips is limited by the effects of multiple scattering. In the TP design, all particle tracks impinge on the Al caps with angles close to 90 degrees. A wall thickness of 100μm would then correspond to about 0.0011 radiation lengths. For the strips the situation is less favourable: all tracks traverse the material at an angle in the range of 0.6 to 17 degrees. Therefore, the effects of multiple scattering are enhanced by a factor in the range of 3.4 to 100. If stainless steel is used, a thickness of 5μm (as is used in Hera-B) is already prohibitive for small-angle particle tracks. Using Al would barely improve the situation since it has less favourable mechanical properties and therefore requires a larger thickness to be used.

- Resistive wall losses might result in excessive heating of the wake field suppressor strips. Note that the strips are so thin that cooling of the strips will be dominated by blackbody radiation, hence the thermal conductivity of the material used is not essential to first order. In addition, resistive heat dissipation itself is (for wall thicknesses smaller than the characteristic skin depth) almost independent of the resistivity of the material used.

- The implementation of such long (1.2m) wake field suppressor strips is difficult. The strips must be connected to the exit window. They must be retractable (by at least 25mm) to allow for beam filling. They must be kept under sufficient tension at all times in order to compensate for inwards displacements of the exit window (during pump-down) and for thermal expansion (see above). Sagging of a strip by more than a fraction of a millimetre could have catastrophic consequences.

- The wake field suppressor strips, being positioned closer to the LHC beams than the rest of the detector setup, will increase the background rates.

- The use of wake field suppressor strips at a few millimetres from the beams, in view of the technical difficulties mentioned above, necessarily introduces a risk for the experiment and for LHC (e.g. sagging, breaking of a strip).

Given the list of problems with the TP design, we have chosen to adopt a solution closer to the “box” design. However one of the complications of the box is that the overlap between upper and lower stations, which is necessary to provide tracking coverage over all azimuthal angles, implies a complex crenulated structure in the box.

Two designs for the crenulation have been considered, a “beampipe” design and a “Toblerone” design. In the beampipe design (Figure 1) the RF shield/box is constructed of two halves, upper and lower. Half-cylinders are impressed in each box. These half-cyclinders resemble a beampipe when the two boxes are together. In order to achieve the overlap between then boxes, and hence the sensors, shallow indentations are made in each box. However, the beampipe design has the problem of presenting substantial material to low angle particles. In order to overcome this it is possible, in a method reminiscent of the TP design, to make the indentations much deeper. Figure 2 shows a view of this Toblerone design. Particles then traverse much less material at low angles. Both designs were considered as options for the new, optimised, design.

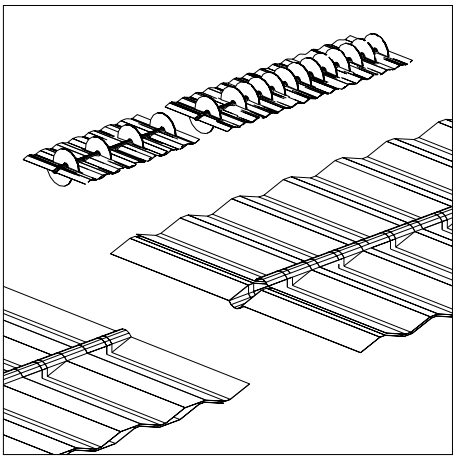

Figure 1: The beampipe RF shield design.

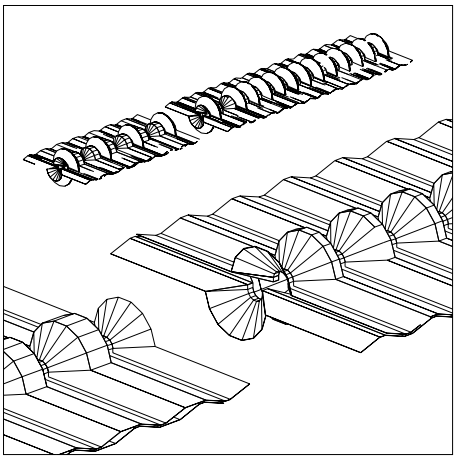

Figure 2: The Toblerone RF shield design.

2.3 Radiation tolerance of silicon

The radiation tolerance of Si detectors has been studied for many current and future experiments, including the ATLAS and CMS experiments at the LHC [8]. Most experiments report the surviveability of "standard" detectors at doses of over 3×10^{14} protons per cm^2. An LHCb prototype detector, fabricated by Hamamatsu, has been irradiated to 3.4×10^{14} protons per cm^2. At an operating voltage of 375V the 300μm thick detector collected over 90% of the deposited charge within the 25ns integration time of the electronics. This is adequate for the VELO. Work is in progress to improve the radiation tolerance of the detectors chosen for LHCb through the use of oxygenated wafers and thinner detectors [9, 10].

For the purpose of optimisation we are concerned only that the detectors are efficient after one year of exposure. Finer details of the fluence in the sensors is dependent on the design, and we refer the reader to Section 4.6, where an evaluation of the flux in our optimised design is presented.

2.4 Sensor dimensions

2.4.1 Outer radius

The inner and outer radius, combined with the spacing between stations, defines the acceptance of the detector. In the Technical Proposal each r and ϕ-measuring plane was construced in two halves which could be separated during injection. In that baseline design each half r and ϕ-plane was composed of 3 overlapping sensors. The segmentation of the detectors was necessary to allow fabrication on a 100mm (4") production line. However, the segmentation implies several undesirable features including complex module assembly and extra material. With 150mm (6") production facilities it is now possible to conceive and design sensors that subtend 180 degrees or more. Although the larger detectors are more difficult to handle than their smaller 60 degree prototypes, the simplicity of the final module design strongly suggests the adoption of 180 degree sensors as a new baseline. The maximum detector radius avail-

able on a 150mm production facility design is about 130mm; on a 100mm production facility about 45mm is the maximum outer radius. The choice of 45mm outer-radius enables us to choose more freely between manufacturers as not all have converted to 6" facilities.

2.4.2 Silicon thickness

The maximum charge that may be collected from a sensor is proportional to the thickness of the detector. A 300μm thick detector will collect the equivalent of 24,000 e^- of charge; if our electronics operated with a noise equivalent to 1000 e^- this would imply a signal/noise ratio for hits of over 20:1. For a detector 150μm thick only about half the signal would be collected, implying either a degraded signal/noise performance or the need for better front-end electronics.

However, using a thick sensor has three undesirable consenquences. First, the amount of material in the detector is increased, leading to more multiple scattering and more secondary particles. This has been modelled below (see Section 4) and thicknesses much above 300μm are shown to be undesirable for the VELO. Second, a thick detector requires a larger operating voltage to provide maximum charge collection [11]. Extremely high voltages are undesirable as this leads to the possibility of breakdown. If a detector cannot be operated at the full voltage required to collect all the charge, the signal/noise will again be degraded. For extreme radiation environments of over 3×10^{14} protons per cm^2 thin detectors of around 150μm are prefered as they limit the operating voltage range to below 300V in most cases. Finally, all detectors have a bulk current. This current not only degrades the signal but in concert with the applied operating voltage gives rise to heating within the sensor. The bulk current depends linearly on the thickness, thus the power dissipated in the silicon is approximately proportional to d^3. Heat must be removed from the sensor to avoid the silicon going into "thermal runaway" and is a critical feature of the choice of operating conditions [12]. In the TP the choice of 150μm sensors was made: a slightly more conservative choice of thickness of 200 to 220μm retains most of the advantages described in the TP and increases the expected signal by over 30$\%$.

Furthermore, the available thickness of the sensors depends strongly on manufacturer and chosen technology. For example, n-strip in n-bulk detectors require more processing on the side opposite the strips than p-strip in n-bulk detectors. This increases the cost of the n-strip option and can also imply a minimum thickness of detector that can be produced (e.g. 300μm).[2]

2.4.3 Strip-pitch

The strip-pitch of a sensor is closely correlated to its "hit" resolution. Assuming normal incidence and no charge sharing between adjacent strips, an ideal detector with pitch w will have a resolution of $w/\sqrt{12}$. Using low-noise analog electronics and the information on charge sharing between strips resolutions closer to $w/12$ are expected. However practical resolution is limited by transverse diffusion, δ-rays and the minimum strip-pitch available for a technology. The minimum pitch differs between different technologies. For n-strip detectors with individual p-stops, as described in

[2] Prototype n-strip detectors in n-bulk of 150μm thickness are available from Micron Semiconductor.

the Technical Proposal, the minimum pitch is $w = 40\mu$m. By using the "older" p-spray technique for isolating the n-strips, or by fabricating a p-strip detector, minimum pitches between 20 and 25μm are available depending on manufacturer.

3 Detector Optimisation

Three of the major changes we investigated were the the sensor thickness, the strip-pitch and the numbers of stations. Below the effect of changing these on the impact parameter and vertex resolution is discussed.

3.1 Impact parameter measurements: strip-pitch and sensor thickness

The L1 trigger uses the VELO data from the r-detectors to determine the primary vertex position, and to find tracks with large impact parameters relative to this vertex. A track in the $r-z$ projection is approximately described by a straight line

$$r = m \times z + b \text{ with } m = \frac{r_2 - r_1}{z_2 - z_1} \text{ and } b = r_1 - m \times z_1, \tag{1}$$

where $r_1(r_2)$ is the measured coordinate of the track in an r-detector at the z-position $z_1(z_2)$. The impact parameter (closest distance of approach) of a track to a given point (r_0, z_0) is

$$IP = \frac{r_0 - mz_0 - b}{\sqrt{1+m^2}}. \tag{2}$$

The error on the impact parameter arises from the intrinsic resolution of the detectors and multiple Coulomb scattering, which in turn depends on the thickness of the material in radiation lengths (x/X_0) and the momentum p of the particle

$$\sigma_{IP}^2 = \frac{\Delta_{01}^2 \times s^2}{p^2(1+m^2)} + \frac{\Delta_{02}^2\sigma_1^2 + \Delta_{01}^2\sigma_2^2}{\Delta_{12}^2(1+m^2)} \text{ with } s = \frac{13.6\text{MeV}}{c}\sqrt{x/X_0}, \tag{3}$$

where Δ_{ij} are the distances between the various points and σ_i the resolution of the measured points. Consideration of these equations leads to two conclusions regarding the design of the VELO.

The first is a natural choice for sensor strip-pitch as a function of radius for the r-detectors. If we require an equal contribution from two measured r-coordinates to the error on the impact parameter then, to a good approximation, $\frac{\Delta_{01}}{\Delta_{02}} = \frac{r_2}{r_1}$. Therefore $\sigma_2 = \sigma_1 \times \frac{r_2}{r_1}$, which suggests a design with the resolution increasing linearly with the radius.

The second is a clear expression for how the impact parameter measurement depends on the resolution and the radius of the first measured point. For low angle tracks ($m < 0.39$) and primary vertices close to the z-axis, equation 3 can be rewritten as

$$\sigma_{IP}^2 = \frac{r_1^2 \times s^2}{p_t^2} + 2f^2\sigma_1^2, \tag{4}$$

with $f = \frac{\Delta_{02}}{\Delta_{12}}$ (the extrapolation factor) and transverse momentum p_t. To obtain a good IP measurement one must strive to keep the first measured point close to the primary vertex and minimise the amount of material that causes multiple Coulomb scattering.

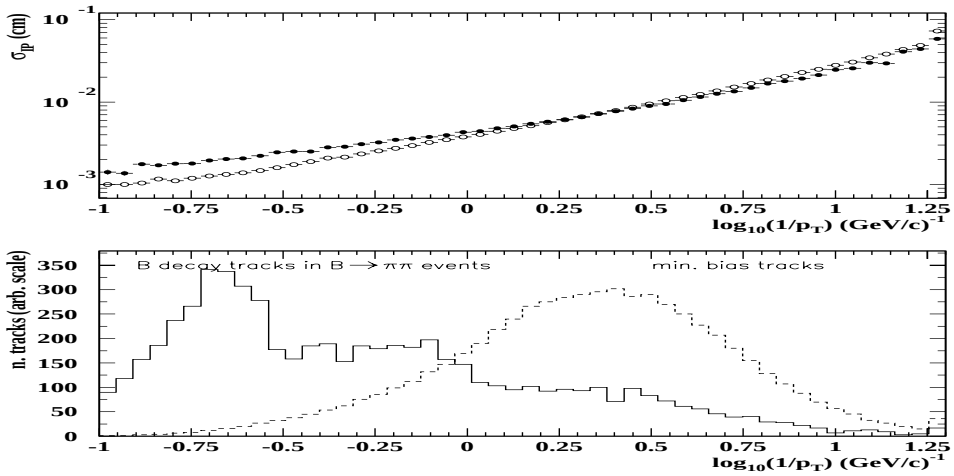

Figure 3: The upper plot shows the error on the impact parameter as a function of $\log_{10}1/p_t$ (p_t in GeV/c) obtained from the full GEANT detector simulation, with the TP (solid circles) and Vb designs (open circles). The lower plot shows the p_t distribution for all tracks from B decays in events where one B decayed into $\pi^+\pi^-$ (solid line), and for tracks from minimum bias events which passed L0 (dashed line).

Note also that in Eq. 4 the contribution from multiple scattering to the impact parameter error depends on the transverse momentum of the particle and not on the total momentum. This is because the measurements are made in the transverse plane only. The error in the longitudinal direction becomes negligible since the position of the detectors will be known very precisely and will be stable during data-taking. This coincides nicely with the fact that tracks from B-decays have on average a larger p_t than tracks from minimum bias events, and so the VELO reconstructs tracks from B-decays with the smallest impact parameter errors (see Figure 3). For tracks with a transverse momentum $p_t > 3$GeV/c, the contribution from the multiple scattering error becomes negligible, and at around $p_t < 2$GeV/c the multiple scattering error starts to dominate. Unfortunately, momentum information is not available at the L1 trigger level. Therefore, the low momentum tracks with large multiple scattering errors are the dominant source for fake large impact parameter tracks.

3.2 Vertex resolution

Secondary vertices may be detected when long-lived particles decay into two or more charged particles. In general the reconstructed tracks will have large impact parameters with respect to the primary vertex. It is to be expected that improving the impact parameter resolution of each track will improve the secondary vertex resolution.

To quantify the dependence of the vertex resolution on detector resolution the LHCb Monte Carlo simulation (SICB [13]) was used with the VELO configuration as described in the Technical Proposal. A B-decay mode, $B \to \pi\pi$, was selected for study and, in order to change the resolution, the sensor strip-pitches for both r and

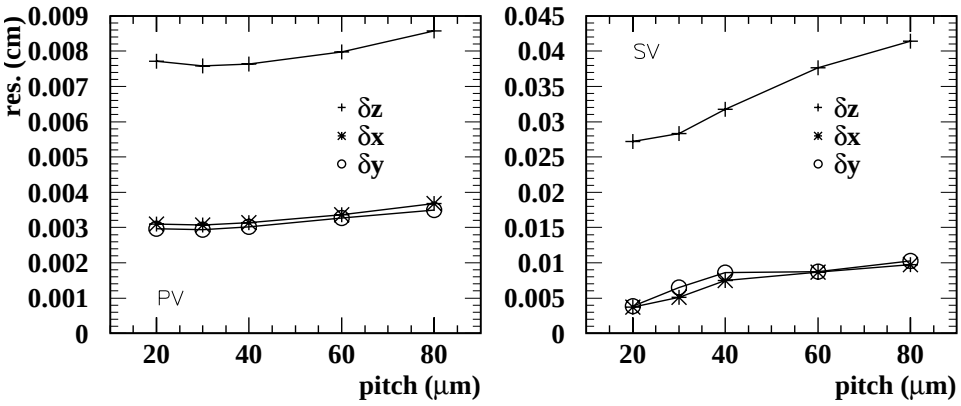

Figure 4: Primary (PV) and secondary (SV) vertex resolutions as a function of strip-pitch for $B \to \pi\pi$ events.

ϕ-measuring detectors were changed in the simulation.[3]

The strip-pitches studied for the inner r and ϕ sectors were 20, 30, 40(TP), 60 and 80μm. The pitch of the middle and outer r sectors were scaled accordingly, i.e. if the pitch of the inner sector is halved the pitches of the other two sectors are also halved. The resolutions were obtained by comparing the reconstructed primary vertex or secondary vertex position with the Monte Carlo truth in the 3 coordinates: x, y and z. The resolution is then defined to be the RMS separation between the generated position and the reconstructed one.

The results are shown in Figure 4. For the primary vertex there is very little variation in the resolution as a function of pitch (doubling the pitch degrades the resolution by $\sim$15$\%$), while halving the pitch has no discernible effect. This is interpreted as reflecting the high multiplicity of the primary vertex, a large error introduced from a single track being diluted by many well measured tracks. For the secondary vertex we have to reconstruct a vertex from as few as two tracks. Here we see a linear dependence of the resolution on strip-pitch. This is as expected if the error on the vertex position is dominated by the intrinsic detector resolution rather than multiple scattering in the detector. Halving the strip-pitch in the detector would increase the resolution on the secondary vertex position by a factor of two.

3.3 Number of stations

The design of the VELO is complicated by the length of the proton bunches. The interaction point of the primary vertex is expected to be described by a Gaussian dis-

[3]To perform this study $B \to \pi\pi$ DST data was read into the SICB v222 program where the CDF files used to describe the strip-pitches had been altered. The code to to produce new digitisations from the raw GEANT hits (vsdigi.F) was rerun and finally the L1 algorithm (vtm1.F) was called again to produce new 2D tracks, 3D tracks and vertices.

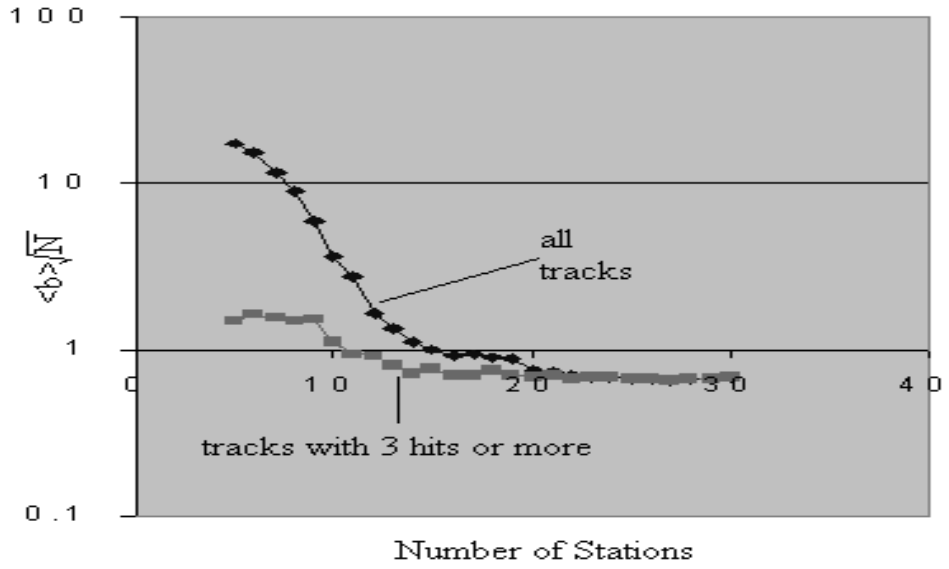

Figure 5: The average impact parameter $< b >$ (arb. units) scaled by $\sqrt{N}$ (where N is the number of stations) versus N for all tracks (upper curve) and tracks with at least 3 hits.

tribution of approximately 80mm FWHM. The detector stations therefore need to be distributed so as to reflect this spread whilst maintaining the required acceptance. This implies the existence of stations upstream of the nominal interaction point. These stations also provide vital information, using "backwards-going" tracks, on the position of the primary vertex.

The number and z-position of the stations depends on several factors: the required acceptance, the minimum number of measured points on a track in the acceptance and the size of the sensors. The optimisation of the position of stations using the full Monte Carlo simulation would be prohibitively time-consuming. Thus, in order to estimate the optimum number of stations, a fast optimisation package was developed. This allowed a sample of tracks either from the PYTHIA [14] generator, or generated uniformly in rapidity, to be propagated through a series of measuring disks. The effects of finite beam spot-size, errors introduced through multiple Coulomb scattering and tracking inefficiencies were simulated. The optimisation was based on moving the z-positions of the stations so as to minimise the average impact parameter of the sample of the tracks.[4] In the optimisation procedure no station was allowed to be closer than 20mm from another.

For 25 stations the results of the z-position optimisation is shown in Table 1. The positions of the stations are not evenly spaced in z, making for a complex design. In addition, the speed of the optimisation was achieved at the cost of not modelling the physics or detailed tracking in the full simulation. Thus we only use the simulation

[4] In order to perform the optimisation meaningfully, a "penalty function" was included which gave tracks with few VELO hits large impact parameters. The arbitrary nature of the penalty function can influence the results.

to indicate the number of stations to be utilised. In Figure 5 the impact parameter scaled[5] by $\sqrt{N}$, where N is the number of stations, is shown as a function of N. For $N < 23$ there are marked improvements in the performance by increasing the number of stations. Much of this improvement is due to the reconstruction of tracks with more than 2 hits. We have chosen to minimise the number of stations whilst requiring there is no significant deterioration to the performance of the detector due to "missed" tracks. To test the effect of increasing the number of stations we have used N=25.

stn.	z (cm)	stn.	z (cm)	stn.	z (cm)	stn.	z (cm)	stn.	z (cm)
1	-17.5	6	-0.6	11	14.7	16	42.5	21	65.1
2	-15.3	7	2.8	12	17.6	17	46.7	22	69.5
3	-12.1	8	6.3	13	21.4	18	50.8	23	73.6
4	-7.5	9	9.9	14	29.1	19	55.0	24	76.7
5	-4.5	10	12.2	15	38.3	20	59.2	25	80.0

Table 1: Positions of the 25 stations from z-optimisation study.

3.4 List of VELO designs tested

Given the design constraints and the list of possible imrovements discussed above, a series of different designs were prepared for study. The main design parameters are listed in Table 2.

The different designs were:

TP This design represents the same detector configuration as described in the Technical Proposal (no wake field suppressor strips included).

thick TP Identical to the TP but with silicon 500μm thick. This was used to study the effect of increasing the material budget due to thick Si.

I Increased number of stations (25), reduced outer radius (45mm), thicker silicon (220μm) but otherwise similar to TP. This is an intermediate design between the TP and the new baseline designs.

Ia Identical to design I but with smaller inner radius (8mm). This forms the basis of all the new (25) stations designs.

II Almost identical to the TP; made to study the effect of the Toblerone RF shield.

III Again almost identical to the TP; this time the beampipe RF shield design was used.

IV With the increased number of stations and reduced inner radius, this design was used to study the effect of introducing smaller strip-pitches (hence higher resolution).

[5]The scaling is performed to explicitly separate the result of improving the resolution by increasing the number of stations.

parameter
Si thickness (d)
inner radius of Si (IR)
outer radius of Si (OR)
number of Si stations (nstat)
TP design RF shield
beampipe design RF shield
Toblerone design RF shield
thickness of Al in RF shield (ALth)
strip-pitch for r-detector inner region (SPir)
strip-pitch for r-detector middle region (SPmr)
strip-pitch for r-detector outer region (SPor)

Table 2: VELO design parameters.

stn.	z (cm)	stn.	z (cm)	stn.	z (cm)	stn.	z (cm)	stn.	z (cm)
1	-17.5	6	-2.5	11	12.5	16	27.5	21	52.5
2	-14.5	7	0.5	12	15.5	17	30.5	22	57.5
3	-11.5	8	3.5	13	18.5	18	33.5	23	62.5
4	-8.5	9	6.5	14	21.5	19	42.5	24	67.5
5	-5.5	10	9.5	15	24.5	20	47.5	25	72.5

Table 3: Positions of upper half-stations in z for the baseline and backup designs. The lower half-stations are shifted by +1.5cm with respect to these numbers.

Va A design close to the final design; this is design Ia with a realistic (Toblerone) RF shield.

Vb Identical to Va but with an improved resolution.

baseline The same as design Vb described above but with the positions of the silicon stations in z as shown in Table 3 (and Figure 6). The stations were moved to facilitate construction of the RF shield.

backup The same as the baseline design, but with a silicon thickness of d=300μm and the strip-pitch as in the original TP design, i.e. a conservative detector choice.

These designs are summarised in Table 4. The beampipe and Toblerone RF designs referred to in the table were taken from the LHCb internal note [7] and implemented in SICB. Along with the standard Al thickness for the RF shield (100μm), 250μm thick Al was also considered. Where the number of stations was increased from 17 to 25 (but not for the baseline and backup designs), the z positions of the first and last stations was kept the same as in the TP and the spacing scaled by roughly 17/25. This spacing is similar (but not identical) to that obtained from the z-position optimisation. Figure 6 shows the z positions of the stations for the TP, Vb and baseline/backup designs, together with the angular regions covered.

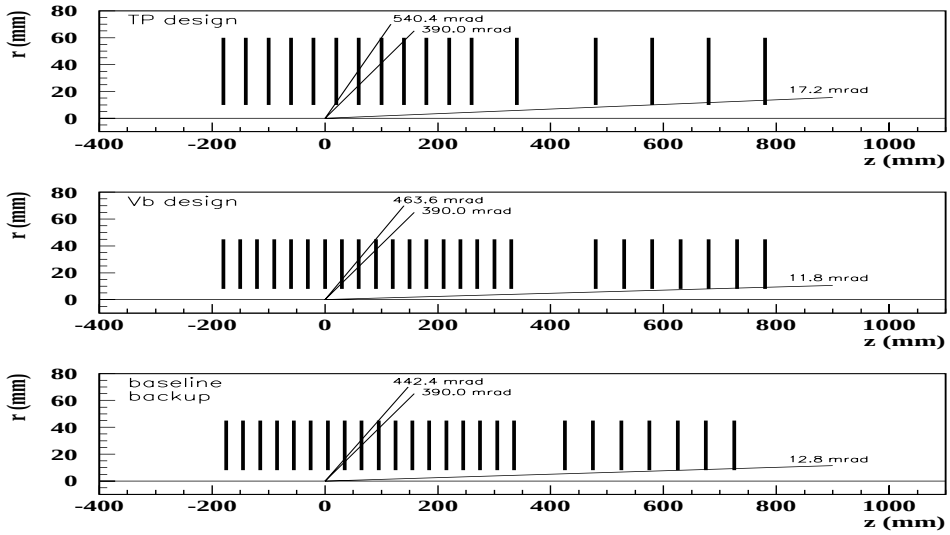

Figure 6: Angular coverage for three VELO designs. The upper and lower limits are for forward tracks which hit at least three stations, while 390mrad signifies the general LHCb acceptance.

VELO design	number stations	silicon parameters d (μm)	IR (cm)	OR (cm)	strip-pitch SPir (μm)	SPmr (μm)	SPor (μm)	RF shield design	ALth (μm)
TP	17	150	1.0	6.0	40	60	80	TP	100 250
I	25	220	1.0	4.5	40	60	80	TP	100 250
Ia	25	220	0.8	4.5	40	60	80	TP	100 250
II	17	220	1.0	6.0	40	60	80	tb	100 250
III	17	220	1.0	6.0	40	60	80	bp	100 250
IV	25	220	0.8	4.5	20	30	40	TP	100 250
Va	25	220	0.8	4.5	40	60	80	tb	250
Vb	25	220	0.8	4.5	20	30	40	tb	250
baseline	25	220	0.8	4.5	20	30	40	tb	250
backup	25	300	0.8	4.5	40	60	80	tb	250

Table 4: VELO designs, with the RF shield design abbreviations: bp=beampipe, tb=Toblerone. See Table 2 for explanation of symbols.

3.5 Simulation methodology

Apart from the fast simulation used to justify the number of stations, all simulation was performed with the full LHCb Monte Carlo program (SICB). Given the number of options that needed to be modelled it was realised early on that a large number of Monte Carlo events would have to be generated to evaluate the performance of the designs. In order to perform these optimisation studies a large 300 PC Linux-based simulation farm was constructed by the Liverpool Group. This Monte Carlo Array Processor (MAP) [15] was commissioned in late 1999 and has generated well over 10,000,000 events for the VELO optimisation.

The simulation code was transferred to Liverpool, from CERN, as an executable. Alterations were made to the source code[6] for the addition of histograms and to define the new RF shield geometries (i.e. the beampipe and Toblerone designs.)

SICB v220/v222			
package	version	files	reason
Finclude	v4r1/v4r2	vrht*.inc	increased stations
		vrpr*.inc	
		vscp*.inc	
		vscr*.inc	
recvdet	v2/v2r1	vrp_r_errors_from_det_sec.F	strip-pitch cluster errors
trivert	v2	vtm1.F, vswo_seq.inc	increased stations
			primary vtx finding (L1)
		vii1.F	initialisation fix
kalman	v2r1/v2r2	matmscm.inc, vsmscm.inc	increased stations
simvdet	v2	vrp_geom_init.F	new RF designs
detdes	v2/v2r1	vsvnam.inc	GEANT names for RF vols
axtrkfit	v2	-	Finclude changes
Futio	v4r1/v4r3	-	

Table 5: Software changes for resolution and event selection studies (SICB v220) and for L1 trigger, multiplicity and other studies (SICB v222).

Furthermore, changes were necessary for the designs with the r-detector strip-pitch halved with respect to that for the TP. For these studies, new cluster errors, used in the track fit, were derived.[7]

[6] More details of the changes are given in Table 5 for the resolution and event selection studies (SICB v220) and for the L0/L1 trigger, multiplicity and other studies (SICB v222). The VELO-specific DDF files also had some array sizes increased, in order to allow for the increased number of stations.

[7] The cluster errors were determined by looking at the difference in position between the true path of the particle as it passed through the silicon and the reconstructed cluster, for each of the three regions of the r-detector. Minimum bias events were used for this study, and the clusters were characterised by whether they consisted of one channel, two channels or more than two channels. As an example, Figure 7 shows this for two-channel clusters; the RMS of these distributions was taken as a measure of the cluster error. Table 6 gives the cluster errors for half-TP strip-pitches, and also the newly-derived cluster errors for the TP design (with the errors derived at the time of the TP in brackets; since the original errors were very close to the new values, they were the ones used in the simulation studies for this note).

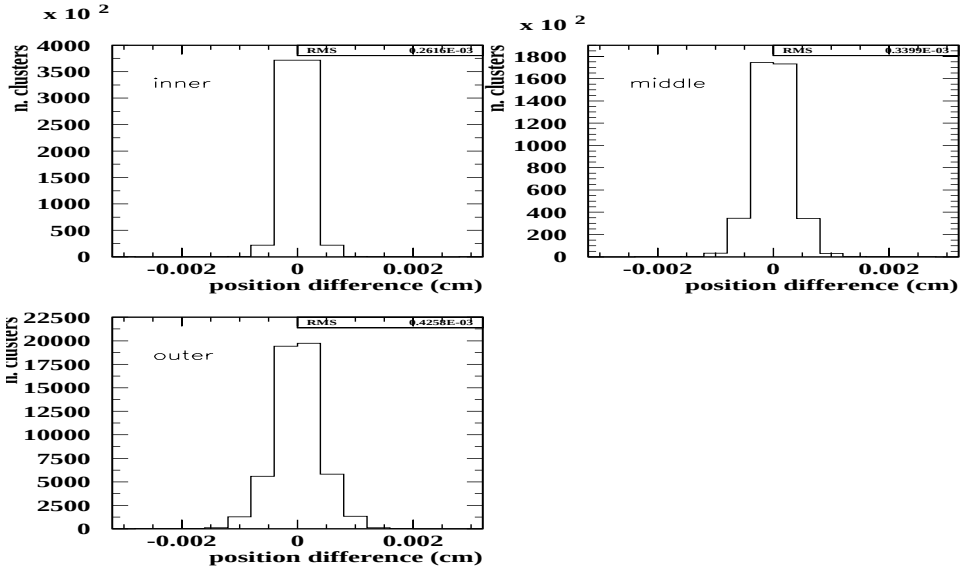

Figure 7: Position differences between true particle paths and reconstructed clusters for three different r-detector regions.

	1 channel		2 channel		>2 channel	
pitch(μm)	RMS(μm)	%	RMS(μm)	%	RMS(μm)	%
20	5.8	46	2.6	44	4.9	10
30	5.9	43	3.4	49	7.0	8
40	7.6	46	4.3	50	10.7	5
40	9.7(9.7)	77	4.6(4.4)	22	26(25)	<1
60	14.6(14.6)	78	7.0(6.7)	21	45(47)	<1
80	19.1(19.0)	79	8.8(8.6)	20	58(56)	<1

Table 6: Cluster errors obtained for half TP (upper) and TP (lower) strip-pitch.

4 Design Evaluation

4.1 Event samples

For the resolution and decay selection studies described in this note, events were generated containing particular B decays, namely $B \to \pi\pi$ and $B \to J/\psi(\mu\mu)K^0_s$. The L0/L1 trigger, particle multiplicity and other studies used minimum bias and $B \to \pi\pi$ events. The total numbers of events for each sample, integrated over the VELO setups, is given in Table 7.

study	event type	n. events	comments
resolution	$B \to \pi\pi$	378k	all θ
	$B \to J/\psi(\mu\mu)K^0_s$	440k	all θ
event selection	$B \to \pi\pi$	771k	all θ
	$B \to J/\psi(\mu\mu)K^0_s$	730k	all θ
trigger, multiplicity	$B \to \pi\pi$	364k	$\theta < 0.6$
and other	minimum bias	987k	$\theta < 0.6$

Table 7: Event samples.

4.2 Measures of performance

Using the event samples, the following quantities were compared to gauge the offline physics analysis and detector performance for each design:

- the RMS of the distribution of the distance between the true primary vertex and the reconstructed primary vertex for each event;
- the RMS of the distribution of the distance between the true secondary (B decay) vertex and the reconstructed secondary vertex for each event;
- the widths of double-Gaussian fits to the distributions of the (true $-$ reconstructed) decay lengths (i.e. the distance between the primary and secondary vertex) and the ratio of the normalisations of the two Gaussians;
- the B decay selection efficiencies and backgrounds using the AXSEL package [16];
- the number of charged and neutral particles per event produced in secondary interactions in the RF shield and detector material as a measure of the effect of any changes in the VELO design on the rest of the LHCb experiment;
- the number of hits per event in the other LHCb detectors as another indication of how VELO geometry changes affect the experiment as a whole;
- the number of VELO hits per track;
- the number of particles per unit area as a function of radius, allowing radiation damage estimates to be made.

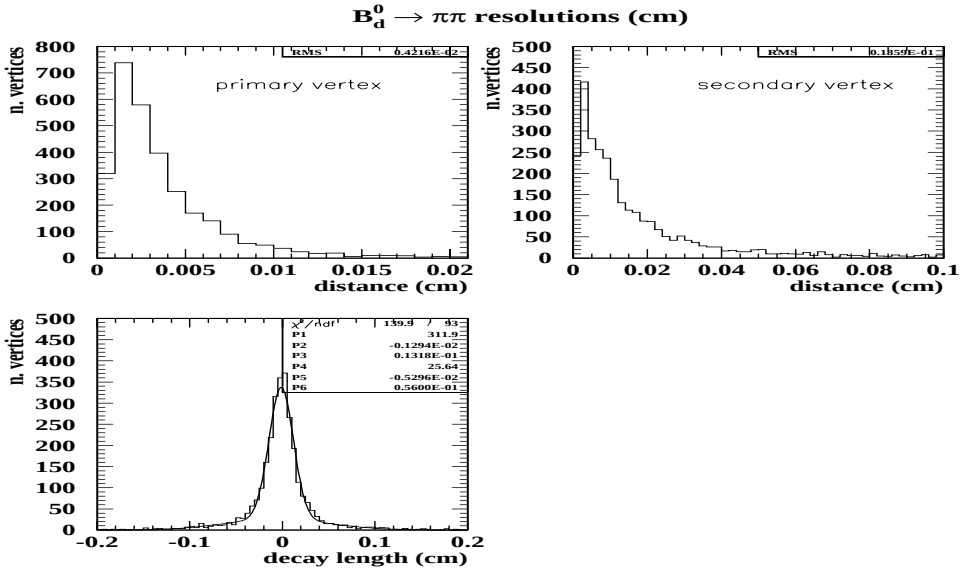

Figure 8: Resolutions for the $B \to \pi\pi$ channel with the TP design; shown are the true $-$ reconstructed vertex position and decay length differences.

The L0 and L1 trigger performances were assessed as follows:

- the L0 algorithm was applied to the events and the efficiencies obtained for each design;
- for the L1 trigger, the average number of reconstructed tracks was compared, both for tracks in the $r-z$ projection (called 2D tracks in the following) and fully-reconstructed 3D tracks; in order to be most sensitive to the trigger performance, the tracks used by the L1 algorithm were used instead of the offline tracks, and cuts were imposed to select b-like tracks;
- the L1 efficiency for $B \to \pi\pi$ events, computed at two different retention levels for minimum bias events, was compared for three different designs of the RF shield.

4.3 Resolutions

Figure 8 gives, as an example, the primary vertex distance and the secondary vertex distance distributions, the RMS of which can be taken as a measure of the resolutions for these quantities, for the $B \to \pi\pi$ channel and for the TP VELO design. Also shown is the decay length resolution, to which a double-Gaussian was fitted.

These plots and numbers were derived for all VELO designs for both the $B \to \pi\pi$ and the $B \to J/\psi(\mu\mu)K^0_s$ channels. The numbers are shown in Tables 8 and 9, and plotted in Figures 9 and 10 (in these and subsequent figures, the order of points in the plots match the order of designs given in the tables; also, A and B on the x-axis signify the baseline and backup designs, tTP the thick Si TP design).

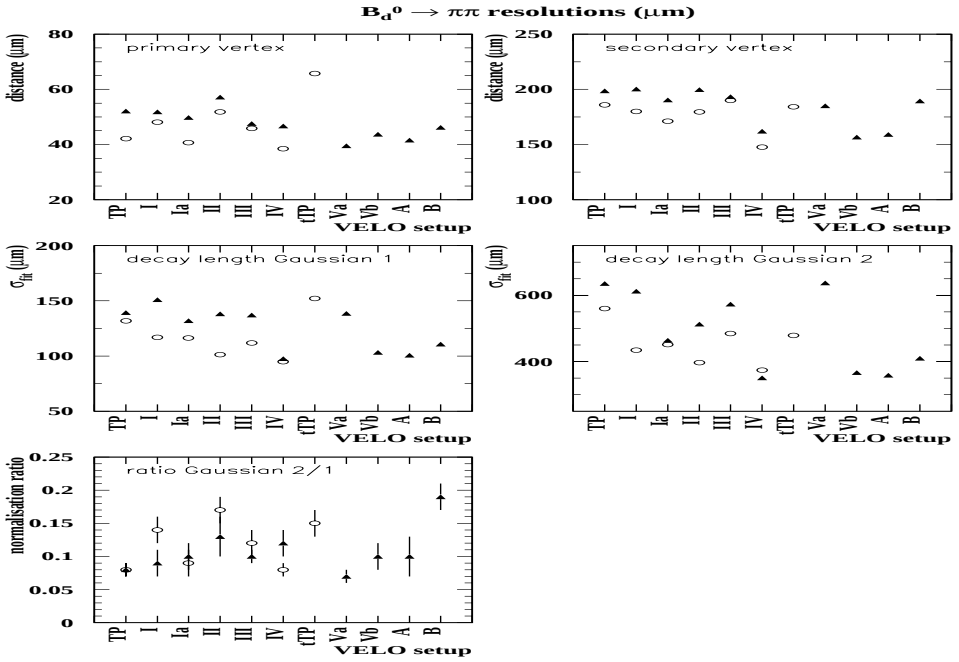

Figure 9: Resolutions for the $B \to \pi\pi$ channel. The circles are for the 100μm Al RF shield, the triangles for 250μm. VELO designs A and B are the baseline and backup designs, tTP the thick Si TP design.

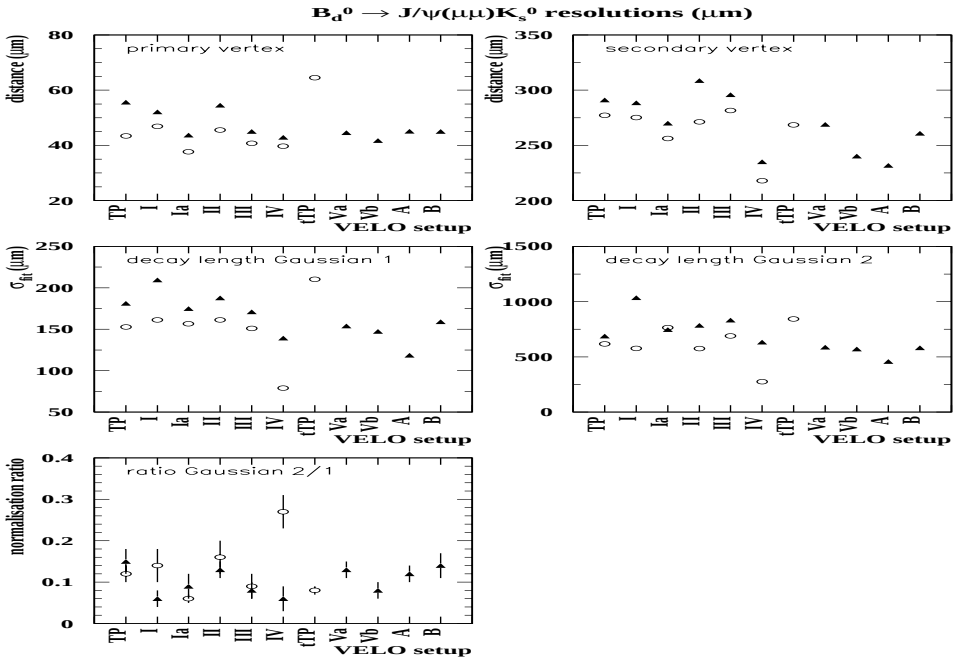

Figure 10: Resolutions for the $B \to J/\psi(\mu\mu)K_s^0$ channel.

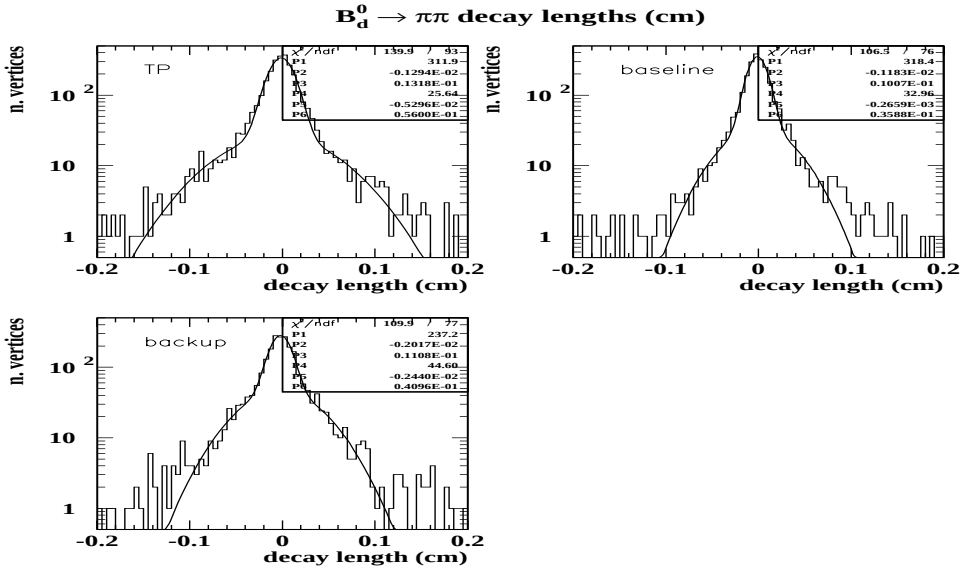

Figure 11: Decay length distributions for the $B \to \pi\pi$ channel, with the TP, baseline and backup designs.

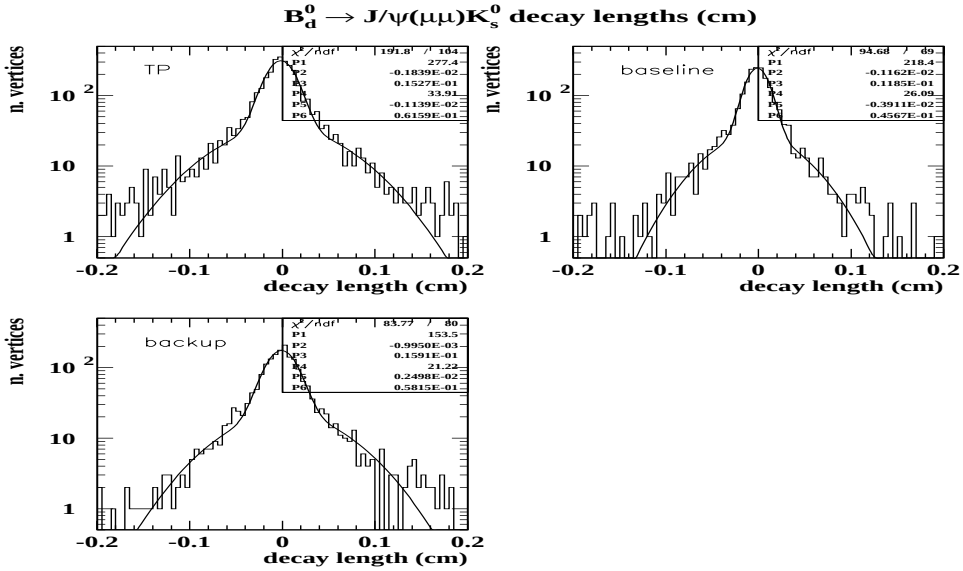

Figure 12: Decay length distributions for the $B \to J/\psi(\mu\mu)K_s^0$ channel, with the TP, baseline and backup designs.

design	RF(μm)	PV	SV	DL1	DL2	DL2/DL1
TP	100	42.2	185.9	131.8	560.0	0.08 ± 0.01
	250	52.1	198.6	139.3	635.6	0.08 ± 0.01
I	100	48.1	179.9	117.0	434.3	0.14 ± 0.02
	250	51.8	200.3	151.0	612.3	0.09 ± 0.02
Ia	100	40.7	171.1	116.4	451.0	0.09 ± 0.02
	250	49.8	190.4	131.9	463.9	0.10 ± 0.02
II	100	51.8	179.5	101.3	397.0	0.17 ± 0.02
	250	57.2	199.7	138.2	512.9	0.13 ± 0.03
III	100	45.8	190.0	111.9	484.6	0.12 ± 0.02
	250	47.6	193.3	137.0	573.3	0.10 ± 0.01
IV	100	38.5	147.7	94.8	373.9	0.08 ± 0.01
	250	46.7	162.0	97.5	350.8	0.12 ± 0.02
tTP	100	65.7	184.2	152.1	478.7	0.15 ± 0.02
Va	250	39.5	185.0	138.6	637.3	0.07 ± 0.01
Vb	250	43.7	156.7	103.3	366.5	0.10 ± 0.02
baseline	250	41.6	159.0	100.7	358.8	0.10 ± 0.03
backup	250	46.2	189.5	110.8	409.5	0.19 ± 0.02

Table 8: Resolutions for the $B \to \pi\pi$ channel, in μm.

design	RF(μm)	PV	SV	DL1	DL2	DL2/DL1
TP	100	43.4	277.1	152.7	615.9	0.12 ± 0.02
	250	55.6	291.0	181.1	688.5	0.15 ± 0.03
I	100	46.9	275.1	161.3	576.3	0.14 ± 0.04
	250	52.1	288.6	209.5	1036.0	0.06 ± 0.02
Ia	100	37.7	256.1	156.7	764.0	0.06 ± 0.01
	250	43.7	270.1	174.9	746.7	0.09 ± 0.03
II	100	45.5	271.3	161.2	573.7	0.16 ± 0.04
	250	54.5	308.6	187.7	785.4	0.13 ± 0.02
III	100	40.8	281.6	150.9	690.2	0.09 ± 0.03
	250	45.0	295.8	171.0	832.0	0.08 ± 0.02
IV	100	39.7	218.0	79.1	273.7	0.27 ± 0.04
	250	42.9	235.1	139.2	632.2	0.06 ± 0.03
tTP	100	64.5	268.6	210.3	844.0	0.08 ± 0.01
Va	250	44.6	269.0	153.9	587.5	0.13 ± 0.02
Vb	250	41.7	240.2	147.2	570.6	0.08 ± 0.02
baseline	250	45.1	231.8	118.5	456.7	0.12 ± 0.02
backup	250	45.0	260.9	159.1	581.3	0.14 ± 0.03

Table 9: Resolutions for the $B \to J/\psi(\mu\mu)K_s^0$ channel, in μm.

The main effects shown in these plots are the decrease in the primary vertex resolution when going to thick (500μm) silicon, and the overall loss of resolution when increasing the thickness of the RF shield. Decreasing the strip-pitch by a factor of 2 leads to an increase in the resolution on the secondary decay vertices and thus the decay length. Furthermore, decreasing the inner radius of the silicon and using the Toblerone design for the RF shield have beneficial effects.

Figures 11 and 12 show for the two B decays studied the decay length distributions, with the double-Gaussian fits, for the TP, baseline and backup designs. The relative importance of the wide and narrow Gaussians, and the number of vertices in the tails, can be gauged.

The resolution results obtained for the optimised z positions for the silicon stations (described in Section 3.3) showed no improvement relative to those for the TP situation (and were in some cases worse), and so are not considered further.

4.4 Event selection efficiencies and backgrounds

Using the event selection package AXSEL, with standard (and thus non-tuned) cuts, the 4π event selection efficiencies were obtained, again for all VELO designs and both the B decay channels considered in the last section. The backgrounds to these selections were also estimated using AXSEL. Both sets of numbers are listed in Tables 10 and 11. Again, for ease of comparison, these numbers are plotted, in Figure 13.

There appear to be no major systematic effects regarding the efficiency and background numbers as the VELO design is varied. Any perceived loss of efficiency or increase in background may well be removed with tuning of the selection cuts.

4.5 Multiplicities and material mapping

Figure 14 shows the number of particles per $B \to \pi\pi$ event as a function z for different regions of r (from the truth information).[8] Distributions such as these were obtained also for minimum bias events. Then the ratios of the number of particles which pass the fiducial cut (3mm$<$ r $<$6cm, -10cm$<$ z $<$82cm) on the (r,z) positions of the

[8]The spikes in the plot for charged particles originating far from the primary vertex are due to electrons and positrons from photon conversions.

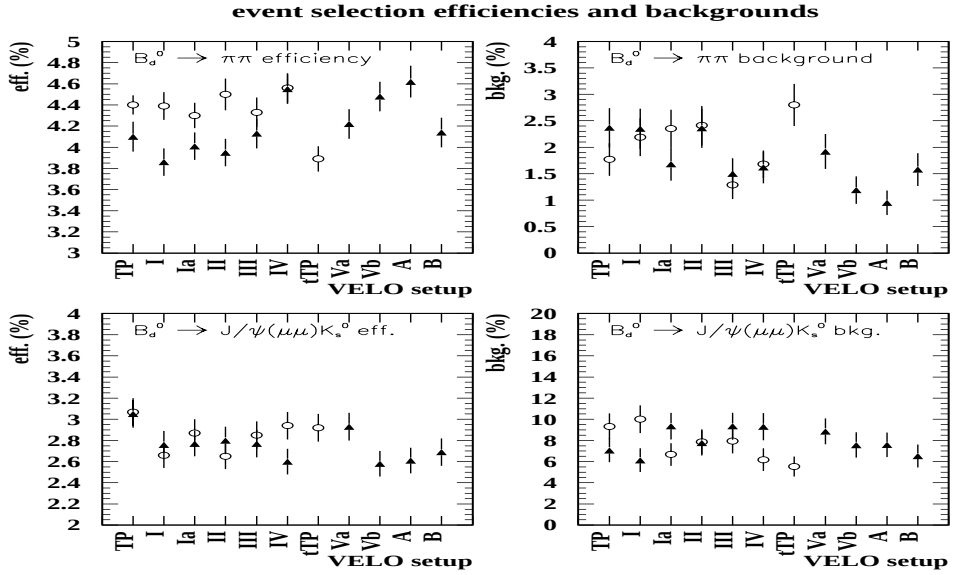

Figure 13: Efficiencies and backgrounds for the $B \to \pi\pi$ and $B \to J/\psi(\mu\mu)K_s^0$ channels.

origin to those which pass the fiducial cut ($r <$ 3mm, -10cm$< z <$82cm), which is roughly constant for each design, were formed. The fiducial cuts cover the region affected by the changes in the VELO design. The multiplicity ratios given in Tables 12 and 13 (and plotted in Figure 15) are for charged and neutral particles, for $B \to \pi\pi$ and minimum bias events respectively.

As expected, the number of secondary particles produced increases as the amount of material in the VELO system increases, be it in the RF shield or in the silicon. The variation is up to a maximum of 8% in the total charged multiplicity and about 0.5% in the total neutral multiplicity.

A different measure of the secondary particle multiplicity was also used: the number of raw GEANT hits in each detector for minimum bias events which passed the L0 trigger (for the HCAL, the number of L0 clusters was used). Distributions of these quantities are shown in Figures 16,17 and 18 for the TP, baseline and backup designs. From these plots and the means given in Table 14, the increase in the number of hits going from the TP to the baseline design is $< 5\%$, varying depending on the detector, and between 5% and 10% going from the TP to the backup design.

4.6 Particle fluxes and radiation damage estimates

In the VELO detector the sensor performance is not uniform but is strongly dependent on the integrated flux of particles at a particular position. The flux is proportional to $1/r^{1.9}$, as can be seen in Figures 19 and 20, which show the distributions for two VELO designs and for $B \to \pi\pi$ and minimum bias events, together with fits to the function $P1 \times r^{P2}$. The flux is approximately independent of the z-position of the detector.

design	RF (μm)	eff.(%)	bkg.(%)
TP	100	4.40 ± 0.09	1.77 ± 0.31
TP	250	4.10 ± 0.14	2.37 ± 0.37
I	100	4.39 ± 0.13	2.19 ± 0.36
I	250	3.86 ± 0.13	2.35 ± 0.38
Ia	100	4.30 ± 0.12	2.35 ± 0.36
Ia	250	4.01 ± 0.13	1.68 ± 0.31
II	100	4.50 ± 0.15	2.41 ± 0.37
II	250	3.95 ± 0.13	2.36 ± 0.37
III	100	4.33 ± 0.14	1.29 ± 0.27
III	250	4.13 ± 0.14	1.50 ± 0.29
IV	100	4.56 ± 0.14	1.68 ± 0.26
IV	250	4.55 ± 0.14	1.62 ± 0.30
tTP	100	3.89 ± 0.12	2.80 ± 0.40
Va	250	4.22 ± 0.14	1.92 ± 0.33
Vb	250	4.48 ± 0.14	1.19 ± 0.26
baseline	250	4.62 ± 0.15	0.95 ± 0.23
backup	250	4.14 ± 0.14	1.58 ± 0.31

Table 10: Efficiencies and backgrounds for the $B \to \pi\pi$ channel.

design	RF (μm)	eff.(%)	bkg.(%)
TP	100	3.07 ± 0.13	9.33 ± 1.22
TP	250	3.05 ± 0.13	7.07 ± 1.12
I	100	2.66 ± 0.12	10.02 ± 1.31
I	250	2.76 ± 0.13	6.14 ± 1.11
Ia	100	2.87 ± 0.13	6.67 ± 1.06
Ia	250	2.77 ± 0.12	9.36 ± 1.26
II	100	2.65 ± 0.12	7.86 ± 1.19
II	250	2.80 ± 0.13	7.77 ± 1.18
III	100	2.85 ± 0.13	7.95 ± 1.16
III	250	2.77 ± 0.13	9.34 ± 1.28
IV	100	2.94 ± 0.13	6.19 ± 1.08
IV	250	2.60 ± 0.12	9.30 ± 1.28
tTP	100	2.92 ± 0.13	5.54 ± 0.94
Va	250	2.93 ± 0.13	8.86 ± 1.22
Vb	250	2.58 ± 0.12	7.57 ± 1.20
baseline	250	2.61 ± 0.12	7.59 ± 1.15
backup	250	2.69 ± 0.13	6.53 ± 1.08

Table 11: Efficiencies and backgrounds for the $B \to J/\psi(\mu\mu)K_s^0$

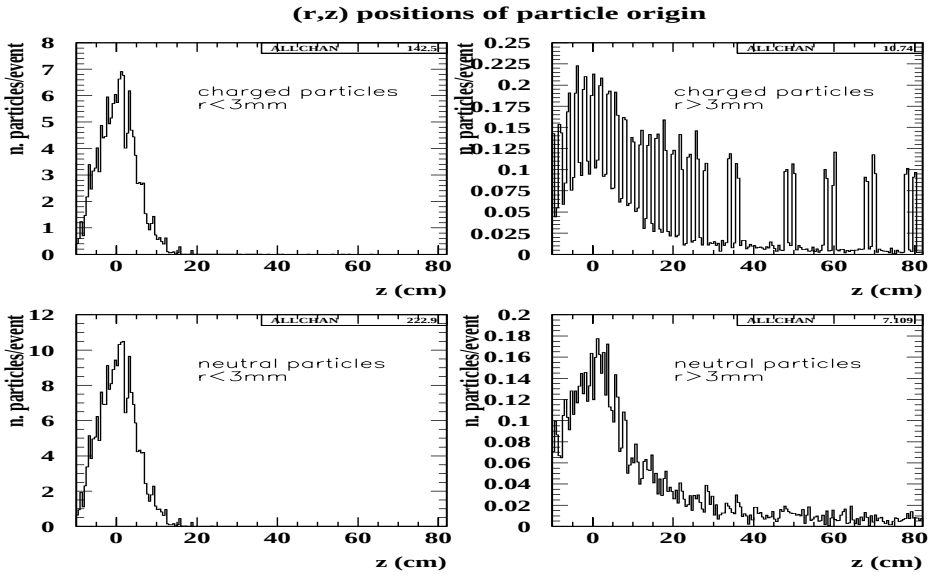

Figure 14: Origin of charged and neutral particles in (r,z) for $B \to \pi\pi$ events.

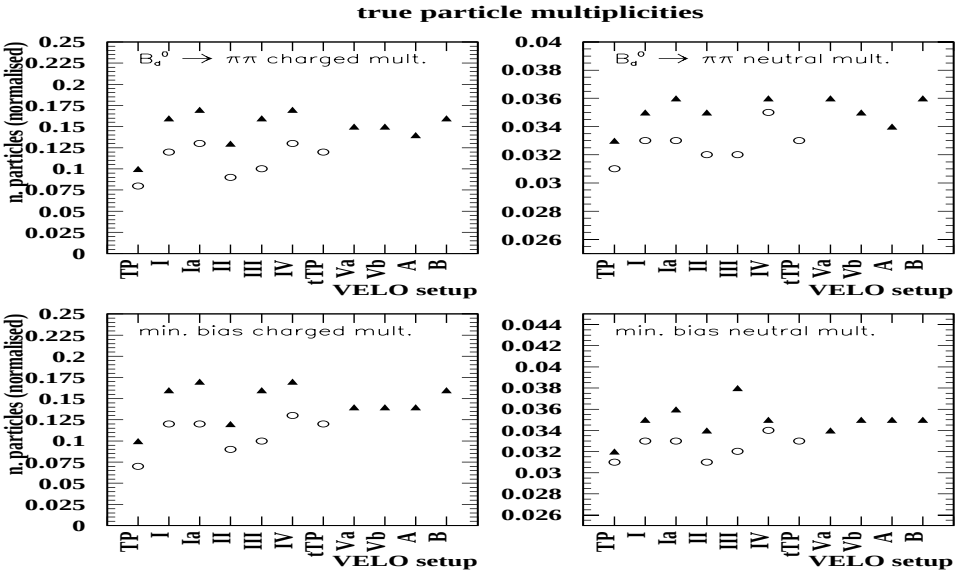

Figure 15: True particle multiplicities for $B \rightarrow \pi\pi$ and minimum bias events.

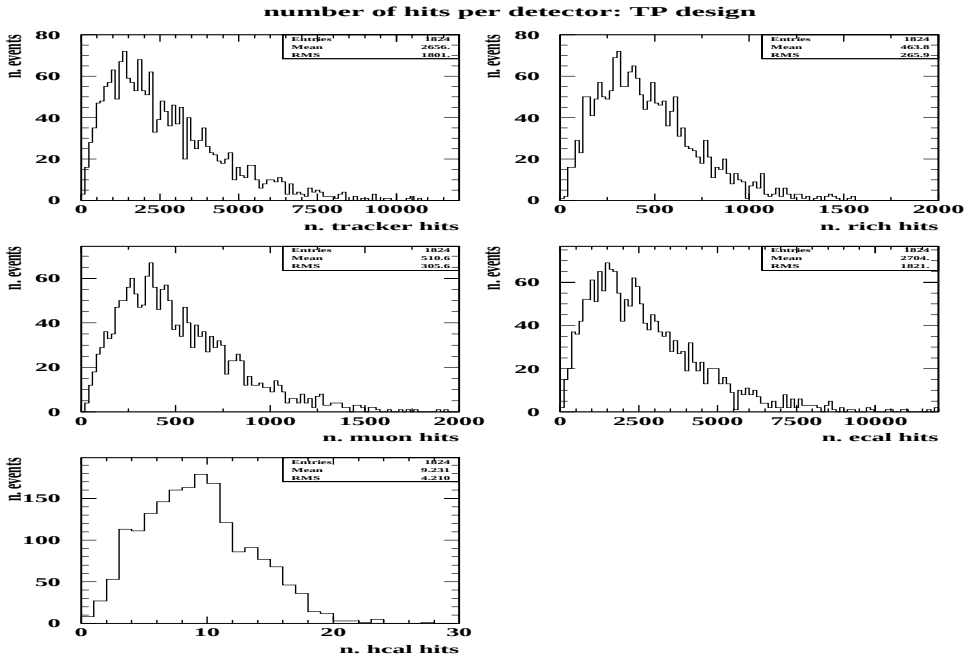

Figure 16: Number of hits per event per detector for the TP VELO design.

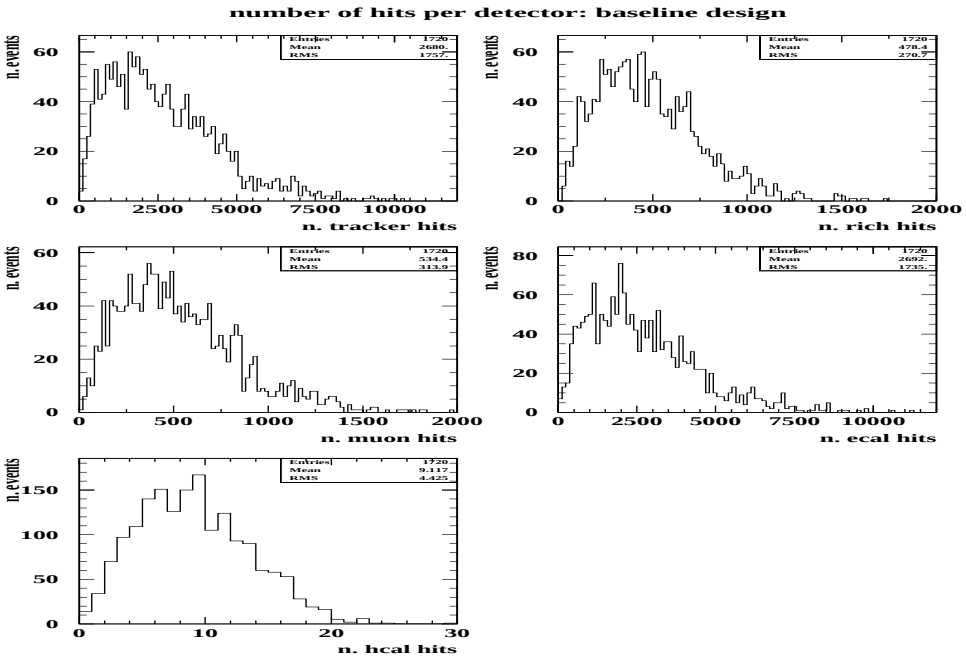

Figure 17: Number of hits per event per detector for the baseline VELO design.

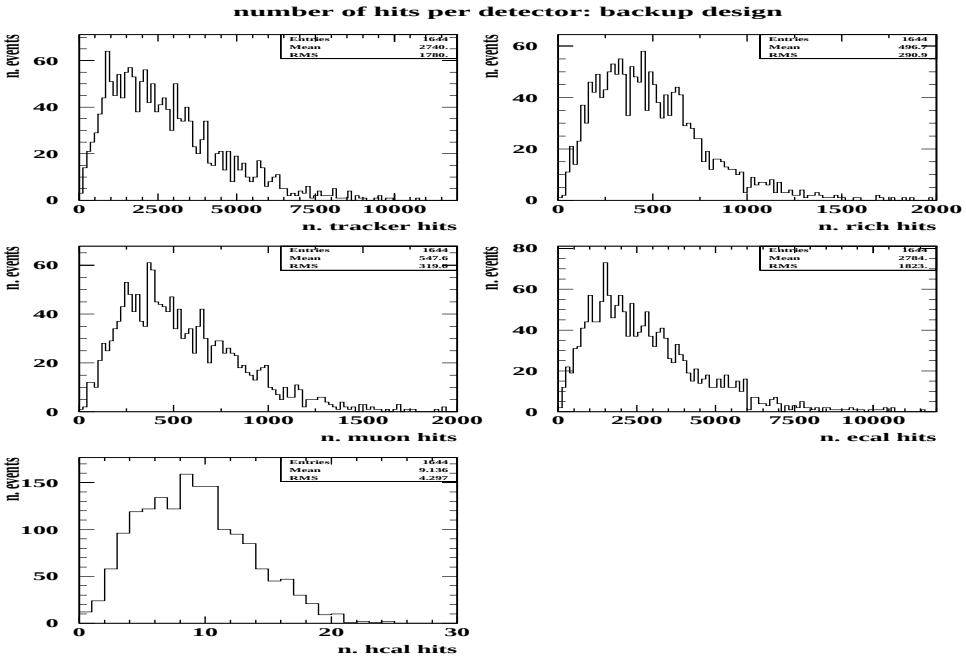

Figure 18: Number of hits per event per detector for the backup VELO design.

design	RF (μm)	ch. mult.	neut. mult.
TP	100	0.08	0.031
TP	250	0.10	0.033
I	100	0.12	0.033
I	250	0.16	0.035
Ia	100	0.13	0.033
Ia	250	0.17	0.036
II	100	0.09	0.032
II	250	0.13	0.035
III	100	0.10	0.032
III	250	0.16	0.038
IV	100	0.13	0.035
IV	250	0.17	0.036
tTP	100	0.12	0.033
Va	250	0.15	0.036
Vb	250	0.15	0.035
baseline	250	0.14	0.034
backup	250	0.16	0.036

Table 12: Charged and neutral multiplicities for the $B \to \pi\pi$ channel.

design	RF (μm)	ch. mult.	neut. mult.
TP	100	0.07	0.031
TP	250	0.10	0.032
I	100	0.12	0.033
I	250	0.16	0.035
Ia	100	0.12	0.033
Ia	250	0.17	0.036
II	100	0.09	0.031
II	250	0.12	0.034
III	100	0.10	0.032
III	250	0.16	0.038
IV	100	0.13	0.034
IV	250	0.17	0.035
tTP	100	0.12	0.033
Va	250	0.14	0.034
Vb	250	0.14	0.035
baseline	250	0.14	0.035
backup	250	0.16	0.035

Table 13: Charged and neutral multiplicities for minimum bias events.

VELO design	tracker	RICH	muon	ECAL	HCAL
TP	2656	464	511	2704	9.2
baseline	2680	478	534	2692	9.1
backup	2740	497	548	2784	9.1

Table 14: Mean number of hits per detector for three VELO designs.

SICB predicts a flux of about one charged particle per cm^2 per interaction at r=1cm, in agreement with the results in the Technical Proposal. Assuming a total inelastic cross-section of 80mb, a luminosity of 2×10^{32}cm^{-2}s^{-1} and 10^7s of operation per year (one LHC year) this represents an integrated flux of charged particles of around 1.6×10^{14}cm^{-2} per year. The majority of these ionising particles are charged pions; the momentum distributions for charged pions in minimum bias events obtained with the PYTHIA generator at r=1cm for stations 7 (z=0.5cm) and 25 (z=72.5cm) of the baseline/backup VELO design are shown in Figure 21. These distributions were folded with the NIEL tables for charged pions ([17] and Figure 21) and the expected displacement damage to the silicon relative to 1MeV neutrons (D/D*) obtained (a value of D/D*=0.37 was assumed for $p > 9$GeV/c). The results are shown in Figure 21 normalised to the number of pions, together with the sums over the bin contents. Thus, the yearly dose at r=1cm is equivalent to (0.6 - 1.1)$\times10^{14}$ 1MeV neutrons per cm^{-2}, which is roughly equal to the estimate made in the Technical Proposal.

For detectors with 8mm inner radius the maximum dose received (close to the beam) is about 50% higher (see Figures 19 and 20). The effect of primary and thermal neutrons was not taken into account in these damage estimates; as was shown in the Technical Proposal, the flux of such neutrons is approximately flat in r and at r=6cm

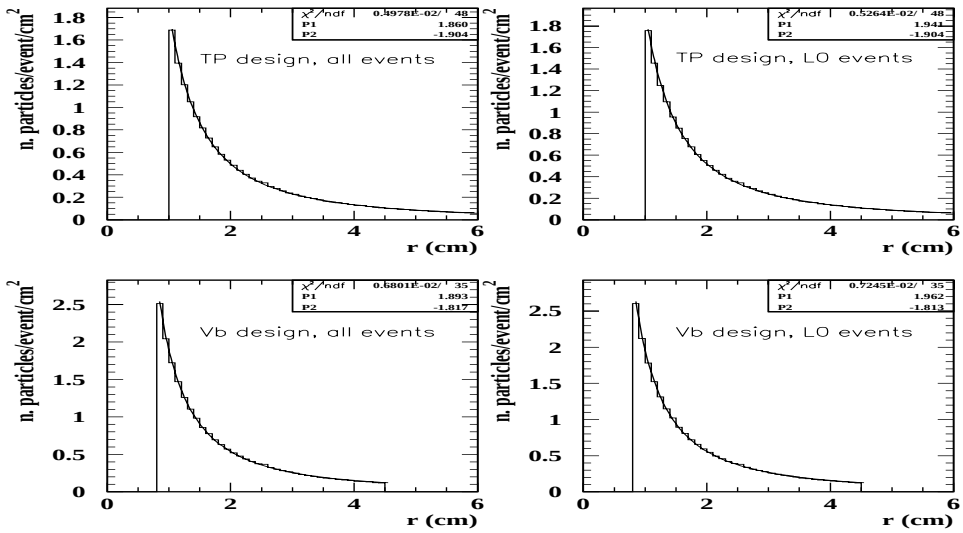

Figure 19: Particle densities on silicon surface for $B \to \pi\pi$ events (all and those which pass L0), for two VELO designs. These plots are integrated over z, so the design with more silicon stations has more entries.

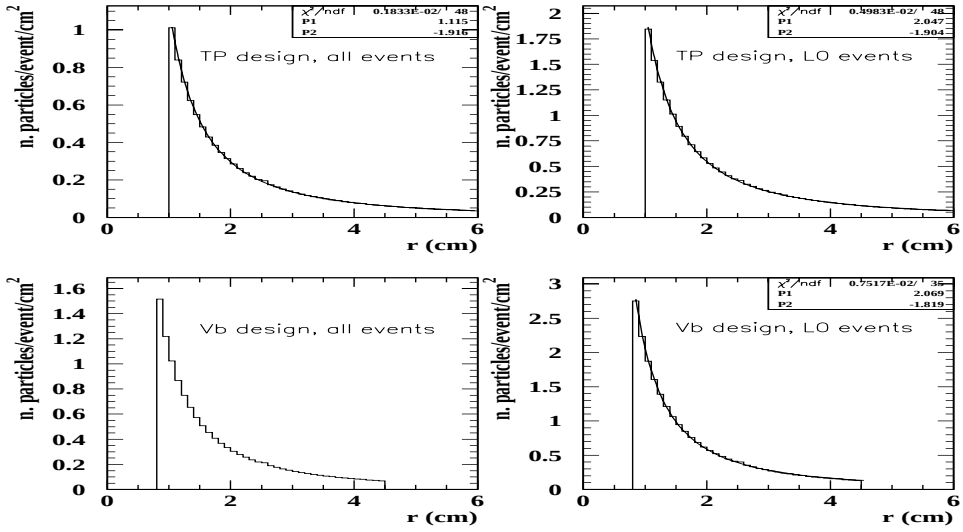

Figure 20: Particle densities for minimum bias events.

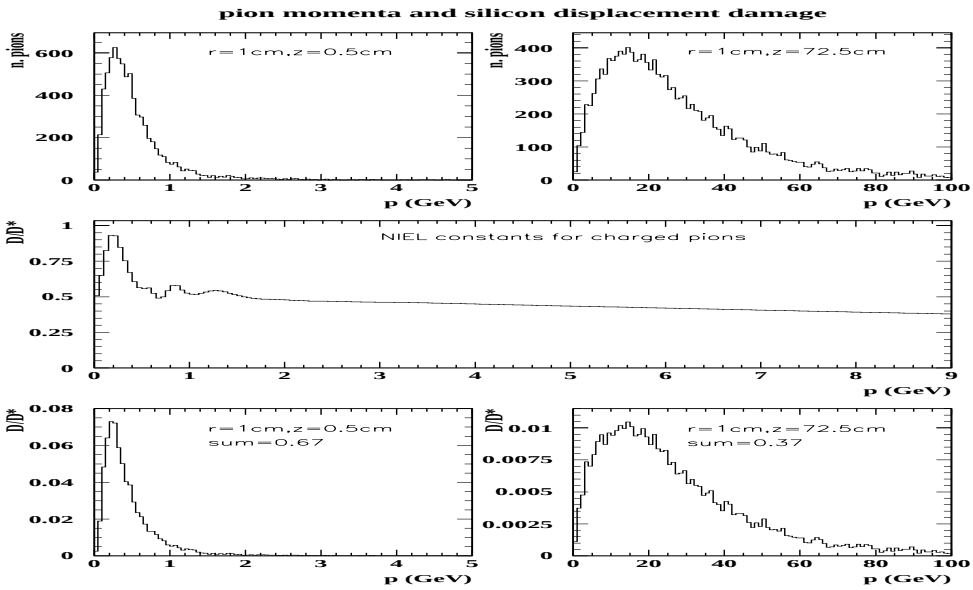

Figure 21: Momentum and D/D* distributions for charged pions in PYTHIA minimum bias events.

makes up about $1/3$ of the total particle flux.

4.7 Number of VELO hits per track

The average number of r and ϕ hits per reconstructed track are shown in Table 15 (and Figure 22) for minimim bias and $B \to \pi\pi$ events, and for two thicknesses of the RF shield. For an increase in the number of stations from 17 to 25 the average number of hits per track rises to over 9. This suggests the VELO may have the increased capability of reconstructing tracks without reference to any other detector.

4.8 L0 trigger performance

The L0 efficiencies obtained for $B \to \pi\pi$ and minimum bias events are shown in Table 16 and Figure 23.

4.9 L1 trigger performance

The L1 trigger relies on the VELO and its ability to reconstruct,and identify, tracks with significant impact parameter with respect to the primary vertex. The trigger performance is strongly dependent on the impact parameter and decay length resolutions. It also depends on the proportion of tracks with high impact parameter which do not originate from b decays. Such tracks mimic the signature of genuine b decays and require the imposition of tighter selection criteria in order to obtain a given trigger rate.

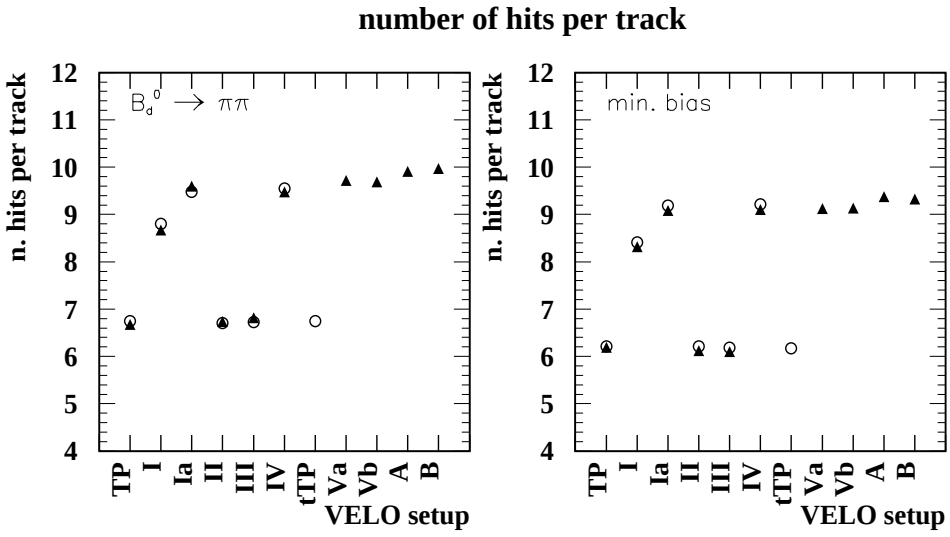

Figure 22: Number of VELO hits per track.

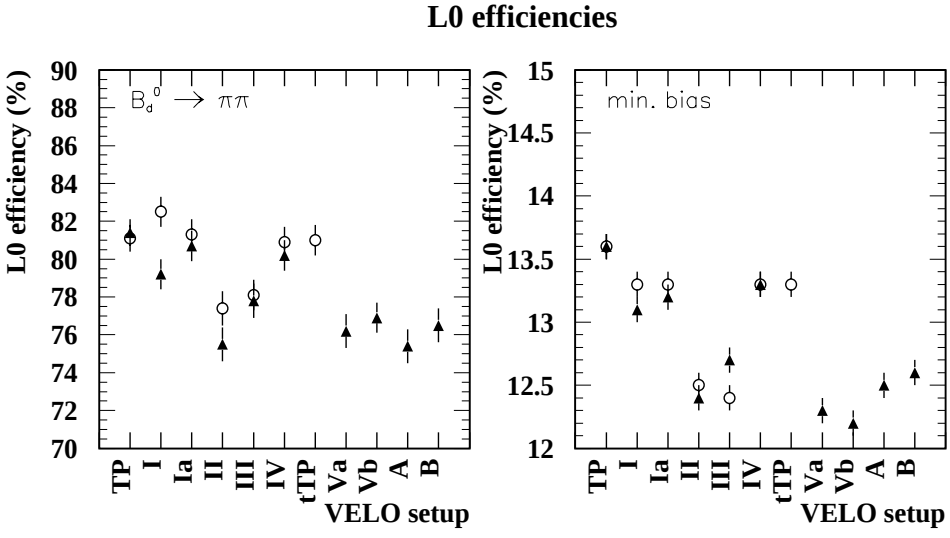

Figure 23: L0 trigger efficiencies.

design	RF (μm)	$B \to \pi\pi$ hits	min. bias hits
TP	100	6.75	6.21
TP	250	6.68	6.19
I	100	8.80	8.41
I	250	8.67	8.32
Ia	100	9.48	9.19
Ia	250	9.60	9.09
II	100	6.71	6.21
II	250	6.74	6.12
III	100	6.73	6.18
III	250	6.82	6.10
IV	100	9.55	9.22
IV	250	9.48	9.11
tTP	100	6.75	6.17
Va	250	9.72	9.13
Vb	250	9.69	9.14
baseline	250	9.91	9.38
backup	250	9.97	9.33

Table 15: Number of hits per track for $B \to \pi\pi$ and minimum bias events.

design	RF (μm)	$B \to \pi\pi$ eff.(%)	min. bias eff.(%)
TP	100	81.1 ± 0.7	13.6 ± 0.1
TP	250	81.4 ± 0.7	13.6 ± 0.1
I	100	82.5 ± 0.8	13.3 ± 0.1
I	250	79.2 ± 0.8	13.1 ± 0.1
Ia	100	81.3 ± 0.8	13.3 ± 0.1
Ia	250	80.7 ± 0.8	13.2 ± 0.1
II	100	77.4 ± 0.9	12.5 ± 0.1
II	250	75.5 ± 0.9	12.4 ± 0.1
III	100	78.1 ± 0.8	12.4 ± 0.1
III	250	77.8 ± 0.9	12.7 ± 0.1
IV	100	80.9 ± 0.8	13.3 ± 0.1
IV	250	80.2 ± 0.8	13.3 ± 0.1
tTP	100	81.0 ± 0.8	13.3 ± 0.1
Va	250	76.2 ± 0.9	12.4 ± 0.1
Vb	250	76.9 ± 0.8	12.3 ± 0.1
baseline	250	75.4 ± 0.9	12.5 ± 0.1
backup	250	76.5 ± 0.9	12.6 ± 0.1

Table 16: L0 efficiencies for $B \to \pi\pi$ and minimum bias events.

For the study of the trigger performance, three different types of tracks were considered:

1. 2D tracks reconstructed in the $r - z$ plane by the L1 algorithm [18].[9]
2. 3D tracks reconstructed by the L1 algorithm. Two sets of 3D tracks were used, one loose selection with impact parameter $d_0 > 50\mu$m with respect to the primary vertex (reconstructed using 2D tracks), and another tighter selection with $d_0 > 100\mu$m.
3. Tracks obtained from the offline reconstruction program. Tracks with momentum larger than $1\,\mathrm{GeV/c}$ and impact parameters with respect to the (reconstructed) primary vertex greater than 50μm or 100μm were selected.

The effect of the impact parameter resolution on the trigger performance was assessed from the average multiplicity of offline-reconstructed particles which passed a given impact parameter cut.

In section 3.1, it was shown that b-like L1 (2D or 3D) tracks in minimum bias events are dominantly found at low momenta, where the impact parameter resolution is dominated by multiple scattering. The average multiplicity of these fake b-like tracks and thus the L1 trigger performance are expected to depend mainly on the amount of material the produced particles traverse before the first measurement point, which in turn varies for the different designs of the RF shield. In order to assess the sensitivity of the trigger algorithm to the geometry of the RF shield, the average multiplicity of b-like L1 (2D or 3D) tracks is compared for designs TP, II and III.

[9] Only those b-like tracks which appear in the L1 summary information ($\log(P_b) > -0.77$, where P_b is the probability of a track to originate from a b decay) were considered.

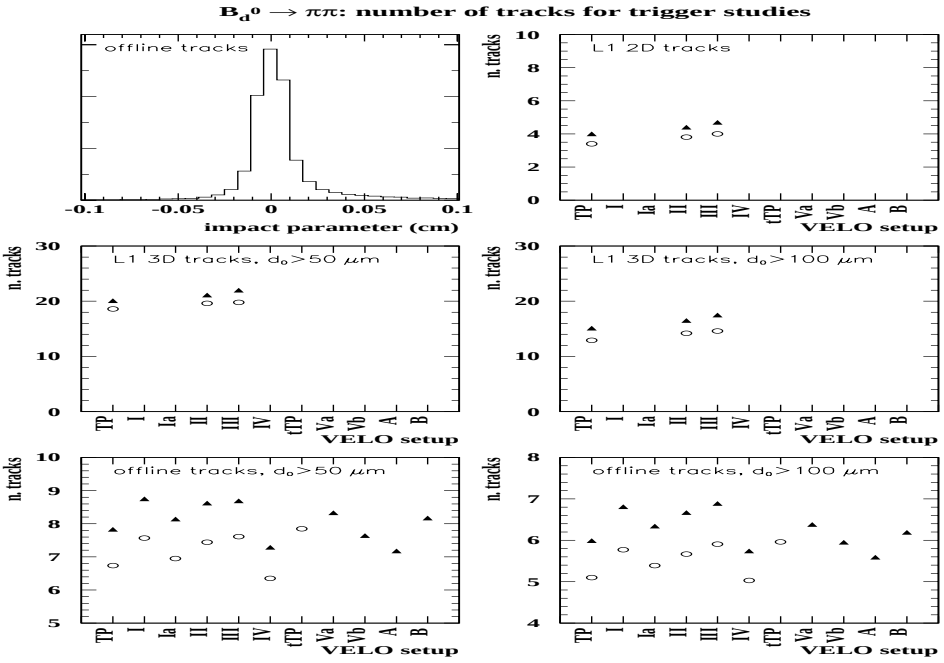

Figure 24: Trigger study track multiplicities for $B \to \pi\pi$ events.

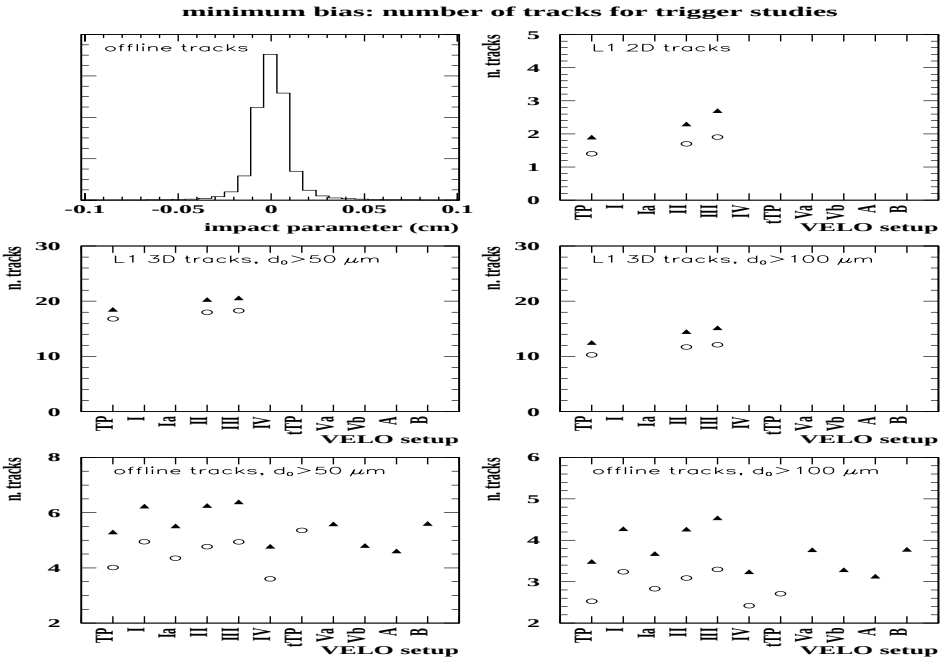

Figure 25: Trigger study track multiplicities for minimum bias events.

$B \to \pi\pi$ events

VELO design	RF shield thickness	L1 2D tracks	L1 3D tracks, $d_0 >$		offline tracks, $d_0 >$	
			$50\,\mu$m	$100\,\mu$m	$50\,\mu$m	$100\,\mu$m
TP	$100\,\mu$m	3.4	18.6	12.9	6.7	5.1
TP	$250\,\mu$m	4.0	20.1	15.1	7.8	6.0
I	$100\,\mu$m	—	—	—	7.6	5.8
I	$250\,\mu$m	—	—	—	8.8	6.8
Ia	$100\,\mu$m	—	—	—	7.0	5.4
Ia	$250\,\mu$m	—	—	—	8.1	6.3
II	$100\,\mu$m	3.8	19.6	14.2	7.4	5.7
II	$250\,\mu$m	4.4	21.1	16.5	8.6	6.7
III	$100\,\mu$m	4.0	19.8	14.6	7.6	5.9
III	$250\,\mu$m	4.7	22.0	17.5	8.7	6.9
IV	$100\,\mu$m	—	—	—	6.4	5.0
IV	$250\,\mu$m	—	—	—	7.3	5.7
tTP	$100\,\mu$m	—	—	—	7.9	6.0
Va	$250\,\mu$m	—	—	—	8.3	6.4
Vb	$250\,\mu$m	—	—	—	7.6	6.0
baseline	$250\,\mu$m	—	—	—	7.2	5.6
backup	$250\,\mu$m	—	—	—	8.2	6.2

minimum bias events

VELO design	RF shield thickness	L1 2D tracks	L1 3D tracks, $d_0 >$		offline tracks, $d_0 >$	
			$50\,\mu$m	$100\,\mu$m	$50\,\mu$m	$100\,\mu$m
TP	$100\,\mu$m	1.4	16.8	10.3	4.0	2.5
TP	$250\,\mu$m	1.9	18.5	12.5	5.3	3.5
I	$100\,\mu$m	—	—	—	5.0	3.2
I	$250\,\mu$m	—	—	—	6.2	4.3
Ia	$100\,\mu$m	—	—	—	4.4	2.8
Ia	$250\,\mu$m	—	—	—	5.5	3.7
II	$100\,\mu$m	1.7	18.0	11.7	4.8	3.1
II	$250\,\mu$m	2.3	20.3	14.5	6.3	4.3
III	$100\,\mu$m	1.9	18.3	12.1	4.9	3.3
III	$250\,\mu$m	2.7	20.6	15.2	6.4	4.5
IV	$100\,\mu$m	—	—	—	3.6	2.4
IV	$250\,\mu$m	—	—	—	4.8	3.2
tTP	$100\,\mu$m	—	—	—	5.4	2.7
Va	$250\,\mu$m	—	—	—	5.6	3.8
Vb	$250\,\mu$m	—	—	—	4.8	3.3
baseline	$250\,\mu$m	—	—	—	4.6	3.1
backup	$250\,\mu$m	—	—	—	5.6	3.8

Table 17: Track multiplicities in $B \to \pi\pi$ (top table) and minimum bias events (bottom table), as defined in the text, for various VELO designs. For L1 2D tracks, a cut $\log(P_b) > -0.77$ was imposed. For offline tracks, $p > 1\,\mathrm{GeV/c}$ was required.

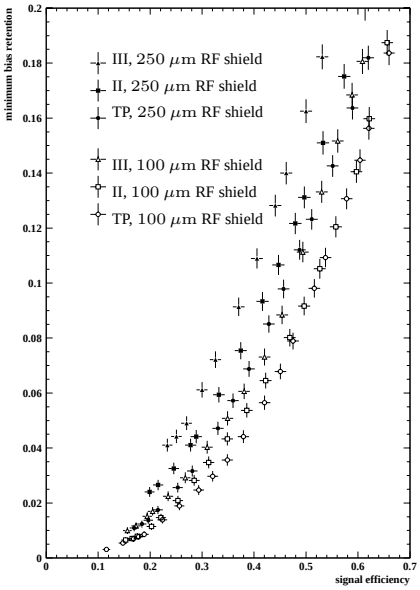

Figure 26: The L1 signal efficiency vs. minimum bias retention curves for various VELO designs, as described in the key to the figure.

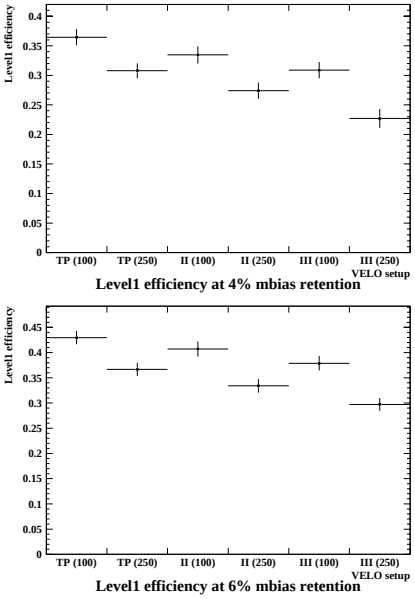

Figure 27: The L1 signal efficiency for various VELO designs, for 4% and 6% minimum bias retention.

The average multiplicities per event are given in Table 17 for $B \to \pi\pi$ and minimum bias events. Plots for these quantities are shown in Figures 24 and 25.

Finally, the overall L1 efficiency as a function of minimum bias retention is computed for $B \to \pi\pi$ events and VELO designs TP, II, and III. In this context, the efficiency is based on events which pass the L0 trigger and, in the case of $B \to \pi\pi$ events, the offline selection. The corresponding curves are shown in Figure 26. In Table 18, the efficiencies for minimum bias retention fractions of 4% and 6% are compared. These numbers are plotted in Figure 27. The numbers at 6% retention are useful when one expects a Super-L1 algorithm to provide part of the rejection power, which would not rely on the vertex detector alone.

An increase of the RF shield thickness from 100μm to 250μm results in a relative L1 efficiency loss of between 15% (TP design) and 27% (beampipe design) for 4% minimum bias retention. In addition, it is observed that a beampipe shaped RF shield results in a poor L1 performance, especially if it cannot be kept very thin.

VELO design	RF shield thickness	signal efficiency at 4% retention	signal efficiency at 6% retention
TP	$100\,\mu$m	$(36.4 \pm 1.3)\%$	$(43.0 \pm 1.3)\%$
TP	$250\,\mu$m	$(30.8 \pm 1.3)\%$	$(36.7 \pm 1.3)\%$
II	$100\,\mu$m	$(33.5 \pm 1.5)\%$	$(40.7 \pm 1.5)\%$
II	$250\,\mu$m	$(27.4 \pm 1.4)\%$	$(33.4 \pm 1.3)\%$
III	$100\,\mu$m	$(30.9 \pm 1.4)\%$	$(37.9 \pm 1.4)\%$
III	$250\,\mu$m	$(22.7 \pm 1.6)\%$	$(29.7 \pm 1.3)\%$

Table 18: The L1 efficiencies for $B \to \pi\pi$ events for three different VELO designs, for 4% and 6% minimum bias retention.

5 Conclusions

A new design for the VELO has been selected. The vertex resolutions for this design are summarised in Table 19; other results of interest, such as the multiplicity of high impact parameter tracks, are shown in Table 20. A backup design with identical geometery but with a more conservative choice of sensor thickness and strip-pitch has also been selected. A comparison of the performance of the new baseline, the new backup and the existing Technical Proposal designs is also shown in Tables 19 and 20. The new baseline design, for the lower station, is shown in Figure 28.

The main features of the new baseline design are:

- The need for increased RF shielding has been met using the Toblerone shape box surrounding the sensors.
- The number of stations has been increased to 25; as a result, the average number of VELO hits per track is 50% higher (around 9.5) leading to a greater standalone tracking capability for the VELO.
- The decay length resolution has been improved.
- The material budget has increased, with a corresponding increase in the number of secondary particles.
- The B-decay selection performance has been maintained.
- The number of high impact parameter tracks (used in the L1 trigger) remains close to the Technical Proposal values.

Acknowledgements

We would like to thank A. Muir, T. Smith and P. Sutcliffe (from the University of Liverpool) and M. Doets, M. Kraan and F. Kroes (from NIKHEF) for work which was vital in the production of this note.

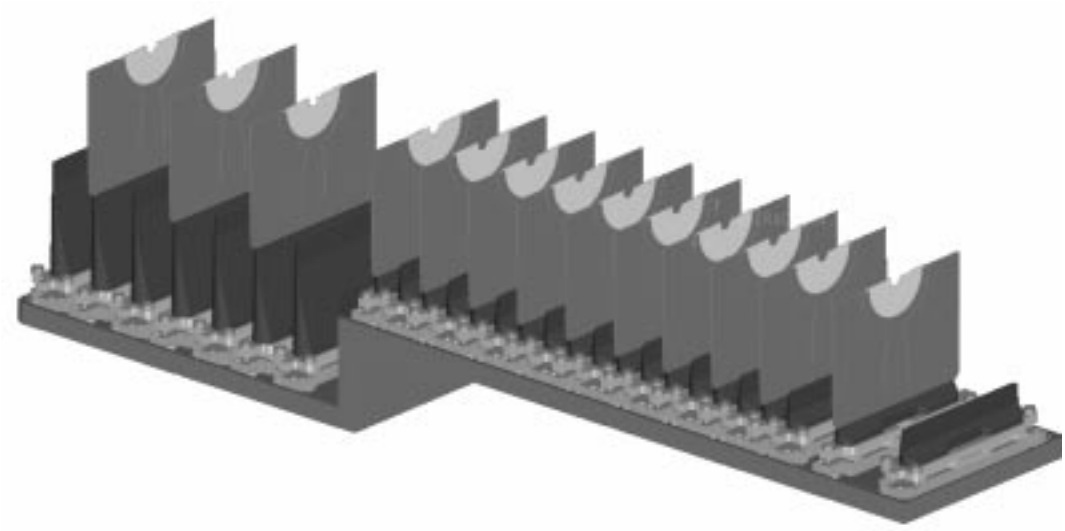

Figure 28: View of the new VELO detector baseline design. For clarity only every second station has its sensor and hybrid shown.

design	channel	PV	SV	DL1	DL2	DL2/DL1
TP	$B \to \pi\pi$	42.2	185.9	131.8	560.0	0.08 ± 0.01
baseline	$B \to \pi\pi$	41.6	159.0	100.7	358.8	0.10 ± 0.03
backup	$B \to \pi\pi$	46.2	189.5	110.8	409.5	0.19 ± 0.02
TP	$B \to J/\psi(\mu\mu)K_s^0$	43.4	277.1	152.7	615.9	0.12 ± 0.02
baseline	$B \to J/\psi(\mu\mu)K_s^0$	45.1	231.8	118.5	456.7	0.12 ± 0.02
backup	$B \to J/\psi(\mu\mu)K_s^0$	45.0	260.9	159.1	581.3	0.14 ± 0.03

Table 19: Vertex resolution comparisons for the TP, baseline and backup designs.

design	channel	ch. mult.	neut. mult.	n. hits	$d_0 > 50\,\mu\mathrm{m}$	$d_0 > 100\,\mu\mathrm{m}$
TP	$B \to \pi\pi$	0.08	0.031	6.75	6.7	5.1
baseline	$B \to \pi\pi$	0.14	0.034	9.91	7.2	5.6
backup	$B \to \pi\pi$	0.16	0.036	9.97	8.2	6.2
TP	min. bias	0.07	0.031	6.21	4.0	2.5
baseline	min. bias	0.14	0.035	9.38	4.6	3.1
backup	min. bias	0.16	0.035	9.33	5.6	3.8

Table 20: Comparisons for the TP, baseline and backup designs.

References

[1] LHCb collaboration, *LHCb Technical Proposal,* CERN/LHCC 98-4.

[2] S. Marti at the *9th International Workshop on Vertex Detectors,* Sleeping Bear Dunes National Lakeshore, MI, USA, September 2000.

[3] M. Doets et al., *Preliminary studies for the LHCb vertex detector vacuum system,* LHCb 99-045 VELO, 15th March 2000.

[4] N. van Bakel et al., *A first study of wake fields in the LHCb vertex detector,* LHCb 99-041 VELO, 21st January 2000.

[5] C. Bauer et al., NIM A447 (2000) 61.

[6] N. van Bakel et al., *Wake fields in the LHCb vertex detector: strip shielding,* LHCb 99-043 VELO, 4th April 2000.

[7] T.J. Ketel, *GEANT description of the aluminium shielding of the vertex detectors,* LHCb 00-019 VELO, 13th March 2000.

[8] S. Walsh at the *3rd International Conference of Radiation Effects on Semiconductor Detectors and Devices,* Florence, June 2000.

[9] G. Casse at the *4th International Symposium on Development and Application of Semiconductor Tracking Detectors,* Hiroshima, March 2000.

[10] D. Robinson at the *8th Pisa Meeting on Advanced Detectors,* Elba, May 2000.

[11] T. Bowcock et al., *Study of the radiation induced charge trapping in irradiated silicon detectors,* LHCb note in preparation.

[12] T. Bowcock and G. Casse, *Operating conditions for the VELO sensor,* LHCb note in preparation.

[13] A. Tsaregorodtsev, *GEANT3-based simulation package for the LHCb experiment,* LHCb collaboration, June 1997.

[14] T. Sjostrand, CERN-TH 7112/93.

[15] T. Bowcock et al., *MAP,* http://www.ph.liv.ac.uk/map/ and at CHEP2000, Padova, February, 2000.

[16] G. Corti, *The AXSEL package,* http://lhcb.cern.ch/ gcorti/analysis/axselect.html/

[17] M. Huhtinen and P.A. Arnio, NIM A335 (1993) 580.

[18] H. Dijkstra and T. Ruf, *The L1 vertex trigger algorithm and its performance,* LHCb 98-006 TRIG, 22nd January 1998.